Nanoscale Horizons

Accepted Manuscript

This is an *Accepted Manuscript*, which has been through the Royal Society of Chemistry peer review process and has been accepted for publication.

Accepted Manuscripts are published online shortly after acceptance, before technical editing, formatting and proof reading. Using this free service, authors can make their results available to the community, in citable form, before we publish the edited article. We will replace this *Accepted Manuscript* with the edited and formatted *Advance Article* as soon as it is available.

You can find more information about *Accepted Manuscripts* in the Information for Authors.

Please note that technical editing may introduce minor changes to the text and/or graphics, which may alter content. The journal's standard Terms & Conditions and the Ethical guidelines still apply. In no event shall the Royal Society of Chemistry be held responsible for any errors or omissions in this *Accepted Manuscript* or any consequences arising from the use of any information it contains.

ROYAL SOCIETY OF CHEMISTRY

rsc.li/nanoscale-horizons

MnO_2 Nanomaterials for Flexible Supercapacitors: Performance Enhancement via Intrinsically and Extrinsically Modification

Teng Zhai, [a,b,] Xihong Lu, [a] Fuxin Wang, [a] Hui Xia, [b,]* and Yexiang Tong [a,]*

([a] *KLGHEI of Environment and Energy Chemistry, MOE of the Key Laboratory of Bioinorganic and Synthetic Chemistry, School of Chemistry and Chemical Engineering, Sun Yat-Sen University, Guangzhou 510275, People's Republic of China. Email: chedhx@mail.sysu.edu.cn.*
[b] *Herbert Gleiter Institute of Nanoscience, Nanjing University of Science and Technology, Nanjing, 210094, E-mail: xiahui@njust.edu.cn*)

Nanoscale Horizons Accepted Manuscript

Abstract

Increasing power and energy demands for next-generation portable and flexible electronics have raised critical requirements (flexibility, stretch-ability, environment friendly, lightweight, *etc.*) to the energy storage devices. Flexible supercapacitors (SCs), as one of the most promising next-generation energy storage devices, have stimulated intensive interests owing to its outstanding features including small size, low weight, ease of handling, excellent reliability, and high power density. Manganese oxide (MnO_2), have attracted a wide range of interests to develop flexible SCs with high electrochemical performance. Yet, the poor electronic and ionic transport in MnO_2 electrodes still limits its promotion in practical applications. This review aimed to describe the recent progresses in MnO_2 materials for flexible SCs, which summarizes the intrinsically modification of MnO_2 via crystallinity, crystal structure, and oxygen vacancy introduction; the extrinsically modification of MnO_2 via non-three dimensional (3D) and 3D flexible conductive scaffold for high performance flexible SCs. Moreover, we also discuss briefly on the current challenges and future directions, opportunities for the development of high-performance MnO_2 based flexible SCs.

Introduction

There has been an increasing demand for fossil fuels originated energy in the past thirty years. However, it may not be possible to provide sufficient of energy as world

population continues to grow and the limited amount of fossil fuels begin to diminish.[1] Sustainable energy sources including solar energy, wind, and tidal energy are emerging as promising candidates to replace the conventional fossil fuel.[2] Since the supply is intermittent and strongly dependent on the natural environment, the development of these sustainable energies has been great limited to their storage. Moreover, the highly efficient, low cost energy storage devices for these kinds of intermittent renewable energies are still one of great challenges. Supercapacitors (SCs), also known as electrochemical capacitors (ECs), have been recognized for more than fifty years and considered as one of the most potential energy storage systems.[3-5] With the rapid growth of electronics, there is increasing demand for flexible or space-saving electronic devices such as wearable electronics, mobile phones, and flexible displays.[6, 7] To catch up with the rapid growth of the demand for portable flexible electronics, it is essential to develop high performance and reliable flexible energy storage devices. In this regard, flexible supercapacitors with high energy density, high power density (high-rate current output/input), and high cycling stability must be able for the practical use of portable flexible electronics. However, it remains a major concern to achieve improved electrochemical performance and ultrahigh flexibility simultaneously.

According to the charge storage mechanism of electrode materials in SCs, it can be generally divided into two categories: electrical double-layer capacitors (EDLCs) and pseudocapacitors.[8] Figure 1 compares the specific capacitances of various types of electrode materials based on these two mechanisms for SCs. EDLCs mechanism based carbon materials store the electrical charge via physical charge separation process, which is strongly dependent on the pore size distribution and high surface area of the carbon materials. In this regard, highly conductive and chemically stable carbon materials with large surface area such as graphene,[9-11] carbon nanotubes (CNTs),[12, 13] activated carbon,[14] have been widely used as electrode materials for EDLCs and achieve specific capacitances of around 50~350 F/g. Due to its conductive electrochemical property and physical storage process, carbon materials based EDLCs can achieve high power (>10 kW/kg) and long term cycle stability

Nanoscale Horizons Accepted Manuscript

(>10^5 cycles). However, it suffers from low capacitance derived low energy density (1~10 Wh/kg). In contrast, conducting polymers or metal oxides based pseudocapacitors can deliver much higher specific capacitance due to that charges are stored via fast and reversible faradic reactions at the surface and bulk of the electrode materials. This will certainly lead to higher energy density (20~50 Wh/kg) in comparison with EDLCs. It should be noted that, due to the slow diffusion of ions within the bulk of the electrode and relative slower charge storage mechanism compared with simple adsorption/desorption, the pseudocapacitors usually possess relatively lower power density (0.5~2 kW/kg). Additionally, it often begins to degrade under less than one or two thousand cycles for reasons of changes in their physical structure and dissolution problems. Therefore, significant efforts have been devoted in the past years on the concerns of pseudocapacitors.

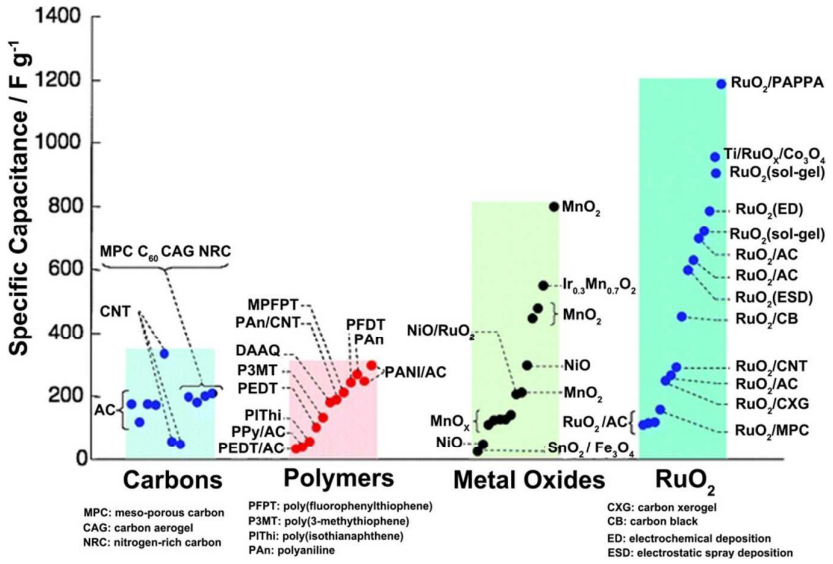

Figure 1 Reported specific capacitances for electrode materials. Reprinted from the ref. [15] with the permission from *Interface*, copyright 2008 - The Electrochemical Society.

Among various pseudocapacitive materials, manganese oxide (MnO_2) is characterized by a low-cost (compared with highly expensive RuO_2) materials with high theoretical capacitance (~1370 F/g) in a wider working potential window (~0.8 to 1 V *vs.* Ag/AgCl in aqueous electrolytes). Over the past decades, MnO_2 has become the most widely investigated pseudocapacitive electrode materials. Latest developments about MnO_2 based supercapacitors have been recently reviewed.[4, 16]

Nanoscale Horizons Accepted Manuscript

However, the practical capacitance is around 200 ~ 600 F/g at mass loading of less than 1 mg/cm^2,[17] so the full potential of MnO_2 for SCs still needs to be further exploited. Intensively explorations have shown that one major issue is crucial for MnO_2 based SCs to achieve fascinating capacitive performance: fast electron and ion transportation in materials or at interface. To solve this problem, considerable effort has been devoted to the crystallinity,[18, 19] crystal structure,[20-24] morphology, nano or micro structural design,[25-31] and vacancies introduction[32-36] of MnO_2 to pursue high-performance MnO_2 based SCs. Fortunately, progress has been made within recent years. Herein, we review these recent progresses in MnO_2 materials for flexible supercapacitors and discuss briefly on the current challenges and future directions, opportunities for the development of high-performance MnO_2 based flexible SCs.

2. Evaluation of electrodes and SCs

Cyclic voltammetry (CV) and galvanostatic charge/discharge (GCD) measurements are two main techniques in SCs to evaluate its electrochemical properties such as specific or areal/volumetric capacitance, rate capabilities, cycling stability, *etc*. Generally, the specific or areal/volumetric capacitance can be calculated via the equation (1) and (2) as follows:

CV curves:

$$C_s = \frac{Q}{m\Delta V} = \frac{S}{2vm\Delta V} \quad (1)$$

GCD curves:

$$C_s = \frac{Q}{m\Delta V} = I\frac{\Delta t}{m\Delta V} \quad (2)$$

Where C_s (F/g) is the specific capacitance; Q (C) is the average charge during the charging and discharging process; m (g) is the mass loading of the active materials; ΔV (V) is the potential window; S (A V) is the integrated area of the CV curve; v (V/s) is the scan rate; I (A) is the constant discharging current; Δt (s) is the discharging time. For areal (C_a) and volumetric (C_v) capacitance, the m in the calculations should be

Nanoscale Horizons Accepted Manuscript

replaced by area (cm^2) and volume (cm^3), respectively.

The average gravimetric power density (P_s) and energy density (E_s) were calculated by using the following equation (3) and (4):

$$\mathrm{E}_s = \frac{1}{2} C_s V^2 \quad (3)$$

$$P_s = \frac{E_s}{\Delta t} \quad (4)$$

Thre corresponding volumertic average power density and volumetic energy density can be obtained by replacing C_s with C_v.

Large values of specific capacitance are always favoured for pursuing corresponding high energy densities. It should be noted that the mass loading and charge/dischare rate are crucial for the evaluation of specific capacitance. High specific capacitance at higher mass loading and higher charge discharge rate, which means high areal capacitance and high output power, is more meaningful for SCs at practical device level. With respect to high energy density, the unquestioning pursuit of large voltage window is also meaningless. High coulombic efficiency, highly stable and reversible reactions in selected voltge window are key parameters for evaluations.

3. High-performance MnO_2 based flexible electrodes

Since the first report about supercapacitor behavior of MnO_2 by Lee and Goodenough in 1999,[37] it has attracted intensively attention and is considered as one of the most promising active materials for SCs due to its high theoretical capacitance (~1300 F/g), low cost, environment friendly features.[38, 39] The high capacitance of MnO_2 is mainly originated from its pseudocapacitance, which can be attributed to the faradic reactions occurring at the surface and subsurface in the bulk of MnO_2 phase. Previous reports [40, 41] indicate that the adsorption/desorption (at surface) or intercalation/deintercalation (at subsurface) of protons and cations are involved in charge storage process, as well as the transition between Mn(*III*) and Mn(*IV*):

Nanoscale Horizons Accepted Manuscript

$$Mn^{III}_{(x+y)}Mn^{IV}_{1-(x+y)}OOC_xH_y \leftrightarrow Mn^{IV}O_2 + xC^+ + yH^+ + (x+y)e^- \quad (1)$$

where C^+ = Li^+, Na^+, K^+. Since both the electrons and ions (protons, and/or cations) are all involved in the charge storage process, it is crucial to achieve high ionic and electronic conductivity in MnO_2 electrode.

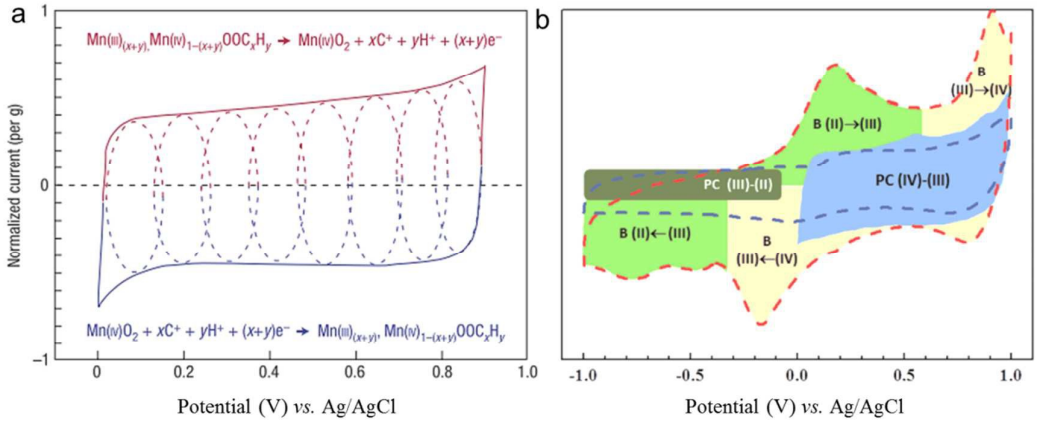

Figure 2. a) Schematic of cyclic voltammetry for a MnO_2 electrode in mild aqueous electrolyte (0.1 M K_2SO_4). The dotted lines highlight the successive multiple surface redox reactions occurring during the charge/discharge process: oxidation from Mn(III) to Mn(IV) accounts for the upper (red) part while the reverse reduction relates to the lower (blue) part. Adapted with permission from ref. [42], copyright Nature Publishing Group 2008. b) Schematic expression of various charge-storage mechanisms as a function of potential; B: battery behavior; PC: pseudocapacitance; (IV), (III), and (II): Mn ions having valences of 4, 3, and 2, respectively. Adapted with permission from ref. [43], copyright Wiley-VCH 2015.

Figure 2a presents the schematic of cyclic voltammetry (CV) for a single MnO_2 electrode in mild aqueous electrolyte (0.1 M K_2SO_4).[42] The dotted lines highlight the successive multiple surface redox reactions occurring during the charge/discharge process in the potential window of 0~1 V *vs.* Ag/AgCl. The oxidation from Mn(III) to Mn(IV) accounts for the upper (red) part while the reverse reduction relates to the lower (blue) part. Clearly, the fast, reversible, and successive multiple reactions takes place all through the potential range of 0~1 V, leading to a well-defined rectangular shaped CV curve (analogous to EDLC behavior). It has been reported that the reversible redox transition of Mn(II)/Mn(III) can also involve in the charge storage process.[4, 43] Very recently, Yu-Ting Weng *et al.* investigated in detail the transitions between Mn(III)/Mn(II), Mn(IV)/Mn(III) within the electrode potential window of

Nanoscale Horizons Accepted Manuscript

-1~1 V *vs.* Ag/AgCl.[43] Figure 2b shows the schematic expression of various charge-storage mechanisms for MnO_2 as a function of potential. At low scan rate of 2 mV/s, the battery behavior of transition between Mn(II)/Mn(III) accounts for ~1/2 of the charge storage. However, the attribution of Mn(II)/Mn(III) decreases sharply when scan rate increases to 100 mV/s, indicating that high ionic and electronic conductivity is the major issue for MnO_2 to achieve fascinating capacitive performance. Unfortunately, the MnO_2 always suffer from poor electronic (10^{-6} to 10^{-3} S/cm) and ionic conductivities, resulting in poor specific capacitance of around 300~400 F/g (~1 mg/cm^2), which is far from its theoretical capacitance of ~1300 F/g.[44, 45]

As reported in the literature in recent years, both the intrinsically modification (crystal structure and crystallinity, microstructural construction, valence introduction) and extrinsically modification (non-3D and 3D carbon, metal oxide based composites) were used to synthesize MnO_2 with improved ionic and electronic property for high performance flexible SCs.

3.1 Intrinsically modified MnO_2 electrode for flexible SCs

3.1.1 Crystallinity and crystal structure

Similar to other transition metal oxide, crystallinity is one of the important factors to intrinsically tune the capacitive performance of MnO_2.[18, 46, 47] MnO_2 with lower crystallinity possesses porous microstructure (higher surface area) and fast ion transportation. However, it will also result in a lower electrical conductivity. Thus, one optimized point with appropriate ion transportation and electrical conductivity can be found via tuning the crystallinity of MnO_2 electrodes. With respect to the crystallinity, the annealing temperature is a common effective approach to achieve optimal electrochemical properties. J. Wei *et al.*[18] annealed the as prepared MnO_2 at 200 °C and found that the calcination lead to the reduced porosity and improved crystallinity. For crystallized MnO_2, series of crystalline structures, including α-, β-, δ-MnO_2 (birnessite), *etc.*, have been investigated in detail. [20-24, 48] Among them, α- and β-MnO_2 possess tunnel structure: mixed of 2×2 octahedral and 1×1 octahedral units

Nanoscale Horizons Accepted Manuscript

for α-MnO_2 (Figure 3a); 1×1 octahedral units for β-MnO_2 (Figure 3a). Figure 3b shows the typical XRD patterns of α-MnO_2 and β-MnO_2. α-MnO_2 shows a pure tetragonal phase [space group: I4/m (87)] with lattice constants a = 9.7847 Å and c = 2.8630 Å (JCPDS 44-0141), while the β-MnO_2 presents a pure tetragonal phase [space group: P42/mnm (136)] with lattice constants a = 4.3999 Å and c = 2.8740 Å (JCPDS 24-0735). It has been reported that the crystalline α-MnO_2 achieved a bulk specific capacitance of ~200 F/g,[41] while the crystalline β-MnO_2 phase exhibited a bulk capacitance of ~ 10 F/g.[23] The tunnel sizes of this two crystal structure are proposed as the explanation for this phenomenon.[49, 50] Until very recently, Matthias J. Young and coworkers [41] present the first time that the detailed charge storage mechanism of α-MnO_2 and explain the capacity differences between α- and β- MnO_2 using a combined theoretical electrochemical and band structure analysis. Figure 3c shows the absolute band edge energies of α-MnO_2 and β-MnO_2 and the electrochemical scanned potential window (SPW) for MnO_2 in aqueous electrolyte at pH of 7.4. The charge-switching states were induced by interstitial cations in α-MnO_2 through stabilization of Mn-O antibonding orbitals from the α-MnO_2 conduction band. Moreover, the cations stabilize high energy dangling O 2p bonds resulting from Mn vacancies. δ-MnO_2 (birnessite), as a 2D materials with open layered structure (inset of Figure 3d), has received intensively attention in recent years.[51, 52] Especially for planar supercapacitors, which enable the entire device to be much thinner and flexible, favors more about quasi-2D graphene like materials.[53-55] Lele Peng and coworkers [22] reported for the first time a high-performance in-plane SC based on hybrid nanostructures of quasi-2D ultrathin δ-MnO_2/graphene nanosheets. Figure 3d shows the XRD pattern of the monoclinic potassium birnessite (JCPDS 80-1098). The peaks of (002) and (006) facets observed in the pattern indicates a well-defined c-orientation, which can facilitates the fabrication of c-oriented thin films. Figure 3e shows the schematic description of the 2D planar ion transport favored within the 2D δ-MnO_2/graphene hybrid structures. The δ-MnO_2 nanosheets integrated on graphene can introduce more electrochemically active surfaces for absorption/desorption of electrolyte ions. Besides, it can also bring additional interfaces at the hybridized

Nanoscale Horizons Accepted Manuscript

interlayer areas to facilitate charge transport during charging/discharging process. The specific capacitance of as prepared planar supercapacitors based on the 2D δ-MnO_2/graphene hybrid at different scan rates (from 50 to 400 mV/s), was shown in Figure 3f. The δ-MnO_2/graphene based planar supercapacitors exhibits enhanced specific capacitance (254 F/g at 0.5 A/g) in comparison with graphene based one (~140 F/g at 0.5 A/g). Furthermore, the former one achieved a better rate capability (~78%, 0.5 to 10 A/g), which is substantially higher than that of graphene-based electrodes (~44%, 0.5 to 10 A/g), confirming the enhanced charge transportation.

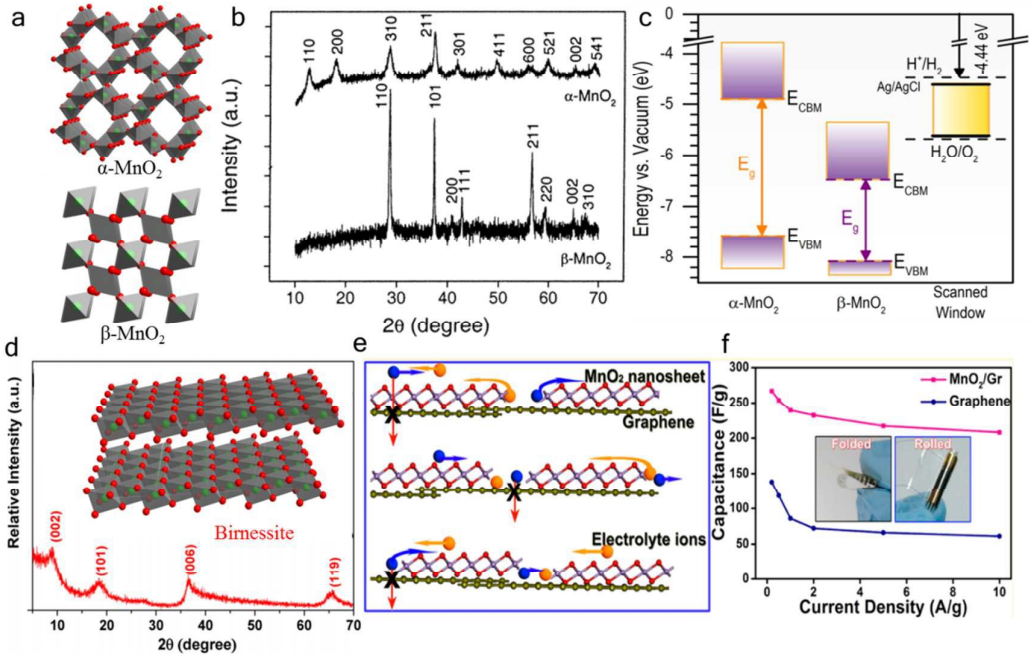

Figure 3. a) Schematic crystal structure of α-MnO_2 and β-MnO_2. b) XRD patterns of α-MnO_2 and β-MnO_2. Reprinted from ref. [104] with permission from Copyright © 2002, American Chemical Society. c) Absolute band edge energies of α-MnO_2 (left) and β-MnO_2 (center) and the electrochemical scanned potential window (SPW) for MnO_2 in aqueous electrolyte at pH = 7.4 (right). Reprinted from ref. [41] with permission from Copyright © 2015, American Chemical Society. d) XRD pattern of the bulk birnessite. Inset is schematic crystal structure of δ-MnO_2 (birnessite). e) Schematic description of the 2D planar ion transport favored within the 2D δ-MnO_2 /graphene hybrid structures. f) Specific capacitance of planar supercapacitors based on the 2D δ-MnO_2/graphene hybrid at different scan rates (from 0.5~10 A/g). Insets show the different bending states (folded and rolled) of planar supercapacitors. Reprinted from ref. [22] with permission from Copyright © 2013, American Chemical Society.

3.1.2 Nanostructural and Microstructural construction

Nanoscale Horizons Accepted Manuscript

Due to the high surface area, the nanostructured MnO_2 electrodes can achieve substantially improved electrochemical performance compared with the bulk MnO_2 electrodes. Thus, the construction of nanostructural MnO_2 electrodes is an effective approach to achieve fast ion transport for MnO_2. Up to now, MnO_2 with various morphologies such as nanorods,[56-58] nanoflower arrays,[59] nanosheets,[19] nanowires,[60] *etc.*, have been intensively reported. Accordingly, the specific surface area of nanostrucetured MnO_2 electrodes are ranging from 20 to 150 m^2/g. Lai and his coworkers [28] synthesized MnO_2 with nanosheets (NS) and nanorods (NRs) morphologies on highly conductive $NiCo_2O_4$-doped carbon nanofibers (NCCNFs). Figure 4a and 4b present the illustration of the electron and ion transport pathways in the $NiCo_2O_4$-NCCNF@MnO_2 NS hybrid membrane and NCCNF@MnO_2 NRs hybrid membrane. The construction of the nanostructured MnO_2 on the surface of NCCNF effectively prevents the MnO_2 nanoparticles from aggregation, which will not only increase its specific surface area but also provide more active sites for the ionic adsorption. Furthermore, Xu *et al.* [25] reported a flexible asymmetric supercapacitor (ASC) based on the MnO_2 nanoflowers @ carbon nano fiber (CNF) cathode nd CNF anode (Figure 4c and 4d).[25] The flower-like MnO_2 material with porous structure enables the fast ion transportation via significantly shorten the diffusion paths, and consequently ensure a high electrochemical performance. A good rate capability, with about 54% retention of the specific capacitance as the current density increases from 3 to 30 mA/cm^2, was achieved by the flower-like MnO_2 on CNF. It should be noted that this value is achieved at a high mass loading of 3.1 mg/cm^2, which is more persuasive. Significantly, the as assembled ASC device also shows outstanding mechanical flexiblity. Figure 4e illustrates that the bending states exert negligible effect on its electochemical properties. Finally, the MnO_2 nanoflowers/CNF based ASC device delivers a maximum energy density of 11.3 Wh/kg at a power density of 352.6 W/kg, which is comparable and higher than other reported values.

Nanoscale Horizons Accepted Manuscript

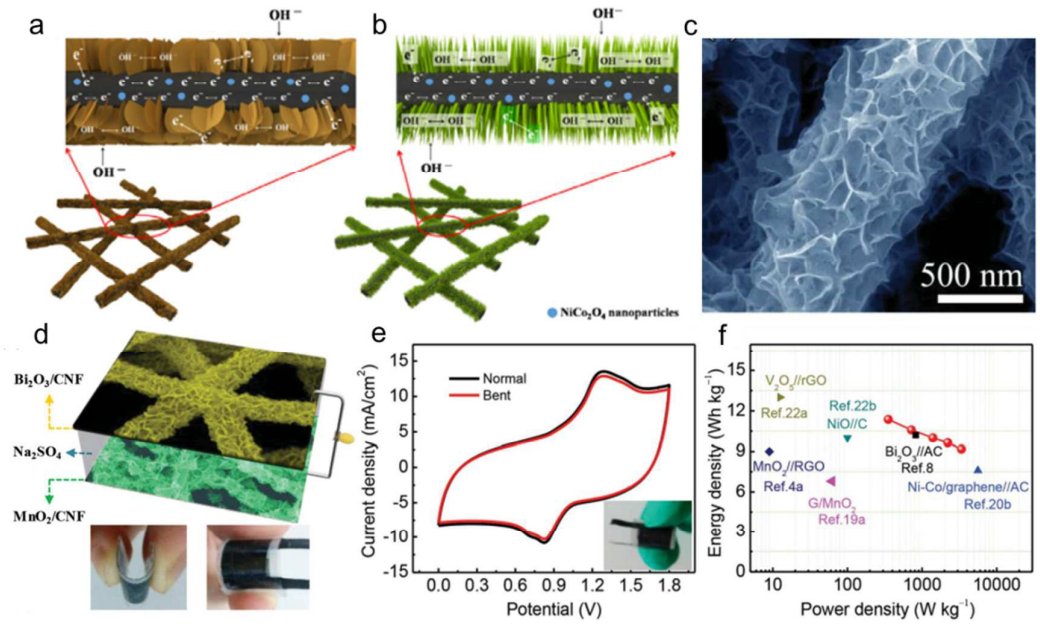

Figure 4. Illustration of the electron and ion transport pathways in the a) $NiCo_2O_4$ -doped carbon nanofibers (NCCNF)@MnO_2 nanosheet hybrid membrane and b) NCCNF@MnO_2 nanorod hybrid membrane. Reprinted from ref. [28] with permission from Copyright © 2015, American Chemical Society. c) SEM image of MnO_2 nanoflowers on carbon nanofibers. d) Schematic illustration of the as-assembled MnO_2 nanoflower based flexible SCs. The digital images present its flexibility. e) CV curves (collected at 200 mV/s) of the as-assembled flexible SCs under flat and bending states. f) Ragone plots of the MnO_2 nanoflower based device. The values reported for other ASCs are added for comparison. Adapted with permission from ref.[25], copyright Wiley-VCH 2015.

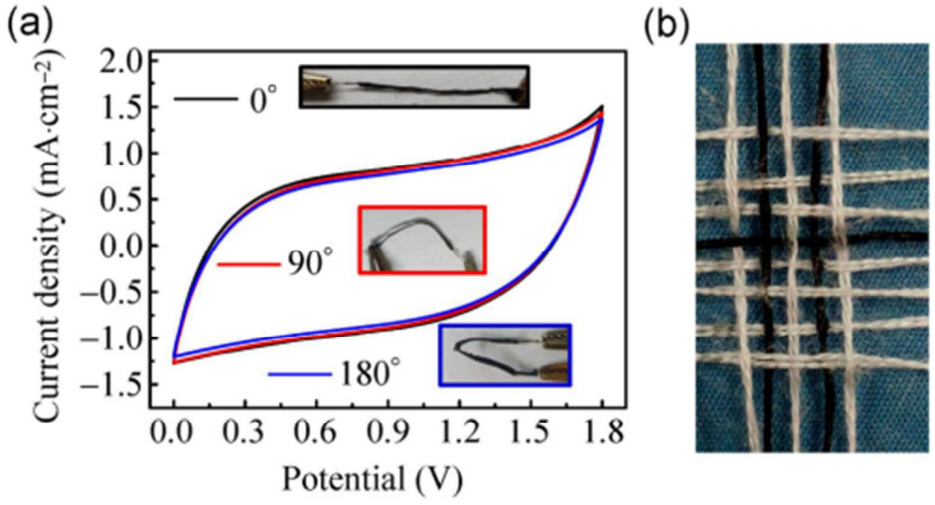

Figure 5. a) CV curves of the fiber-shaped ASC device under different bending states collected at a scan rate of 100 mV/s. Insets are the photo images of device with different bending states (0°, 90°, 180°). b) Photograph of the fiber-shaped device integrated with conventional cotton yarns. Reprinted from ref. [31] with the permission from the Tsinghua University Press and Springer-Verlag

Nanoscale Horizons Accepted Manuscript

Berlin Heidelberg 2014.

As well as the nano-structured construction of MnO_2 materials, the micro-structured construction of MnO_2 electrode is another effective method for MnO_2 to achieve fast ion transport during the charge storage process. The fiber or wire based SCs have been considered to possess distinct advantages over the planar counterparts in the development of reconfigurable, lightweight, and portable electronics.[30, 61-63] Significantly, a wire-shaped device can be co-woven with the well-developed textile technology.[64] Xu *et al.*[31] fabricated an all-solid-state fiber-shaped ASC via wrapping a conducting carbon paper on a MnO_2 nanoflower coated nanoporous gold wire. The MnO_2 nanoflower coated nanoporous gold wire electrode exhibits outstanding capacitance retention of ~88.2% as the current density increase from 0.5 to 8 mA/cm^2, indicating its highly electronic and ionic conductivities. Figure 5a shows the CV curves of the as fabricated fiber-shaped ASC device under different bending states collected at a scan rate of 100 mV/s. Negligible electrochemical performance changes can be observed for the shape-device under different bending states (0°, 90°, 180°). Moreover, the devices are woven into textile structures to show the great potential for future flexible electronic devices (Figure 5b).

Aiming at applications in wearable electronics, the stretch ability has become an important factor for flexible fiber shaped SCs. However, the stretchable fiber shaped SCs are still rarely reported or suffering from low capacitance, low working potential (usually 0.8 V).[65-67] Until very recently, Xu and his co-workers [30] assembled a stretchable fiber shaped ASCs constituted of MnO_2/CNT hybrid fiber positive electrode, CNT fiber negative electrode and KOH-PVA electrolyte (Figure 6a). By taking advantage of the stable working potential of MnO_2/CNT fiber positive electrode (0 ~ 0.5 V *vs.* Ag/AgCl) and CNT fiber negative electrode (-0.4 ~ -1 V *vs.* Ag/AgCl), the voltage window of as assembled ASC device was extended to 1.5 V. High specific capacitance of ~157.53 μF/cm at 50 mV/s was delivered in an extended voltage window of 0~1.5 V. Remarkably, a cyclic tensile strain of up to 100% presents negligible effects on the electrochemical performance of the stretchable ASC device.

Nanoscale Horizons Accepted Manuscript

As shown in Figure 6b, the redox peaks are still well maintained at different tensile strains (0%, 40%, 70%, and 100%) and even after 20 mechanical stretching-releasing cycles (MSRCs), indicating the negligible effects of stretch states to the capacitive performance. The minor capacitance change for the stretched ASC device at varied scan rates again confirms its highly stretch ability (Fig. 6c). Moreover, the specific capacitance still retains more than 99% after 10000 galvanostatic charge/discharge cycles, indicating the long cycling stability.

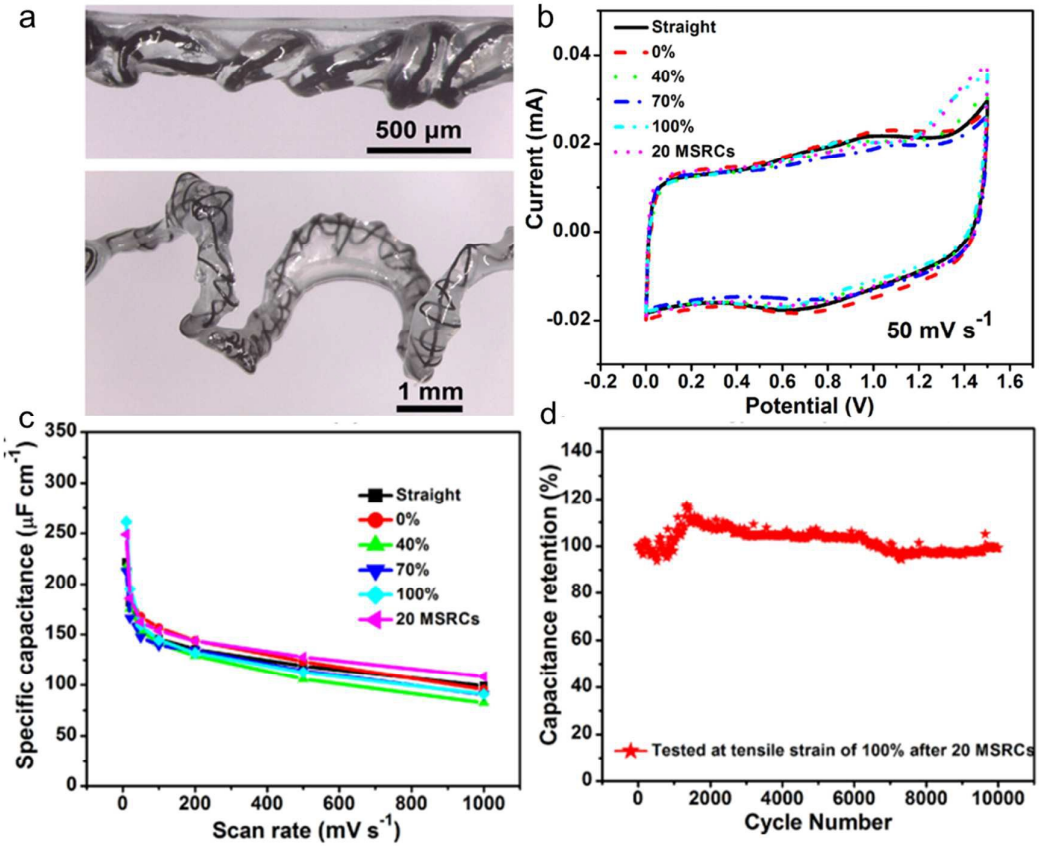

Figure 6. a) Photo images of the as assembled stretchable ASC device. b) CV curves at different stretching states. (c) Specific capacitance variations with scan rates. (d) Cycling performance of the asymmetric supercapacitor at current density of 2.8 mA/cm^2 after 20 MSRCs. Reprinted from ref. [30] with permission from the Copyright © 2015, American Chemical Society.

3.1.3 Oxygen vacancy introduction

The introduction of oxygen vacancy into MnO_2 is believed to be helpful for improving the conductivity and charge storage, and thus enhancing its

Nanoscale Horizons Accepted Manuscript

electrochemical performances.[68-70] The presence of oxygen vacancies in MnO_2 would lead to the charge compensation by changes of oxidation states of Mn ions (Mn^{2+}, Mn^{3+}, Mn^{4+}), which will further result in variation of charge carrier density and make the deficient MnO_2 more conductive.[105-106] Moreover, Song *et al.* [69] performed in situ X-ray absorption near edge spectroscopy (XANES) and density functional theory (DFT) calculations to gain insights of charge storage mechanisms of mix-valent MnO_x. Due to the Mn^{3+} 3d and the O 2p orbitals, excess negative charges can be spilled onto the neighboring O atoms, which means more charges can be stored in deficient MnO_2. In recent years, the researchers have developed two major strategies to introduce oxygen vacancy into MnO_2. The first one is atomic doping with lower valence state impurity.[71-74] Chen *et al.* [75] proposed a strategy to facilitate the formation of oxygen vacancies in ramsdellite-MnO_2 (R-MnO_2) via the introduction of lower valence-state doping, which is effective to enhance the conductivity and activity of R-MnO_2. Figure 7a shows the charge density difference of (010) and (110) surfaces of Zn-doped ramsdellite-MnO_2 with the oxygen vacancy, presenting that the oxygen vacancies are positively charged, and the electrons transfer to near Mn or Zn atoms. Consequently, the charged surface Mn atoms will serve as active sites with better chemical activities. Moreover, the dangling bonds density by coordinately unsaturated Mn will increase as the coordination number of Mn atoms near the vacancies decrease, which will enhance the surface activity.[76] In a word, as shown in Figure 7b, enhanced electrons diffusion to the surface can be achieved by the bulk Zn dopants. The surface oxygen vacancies will draw the electrons to the reaction sites, in where the oxygen vacancies and reduced Mn ions will improve the activity of the electrode reactions in SCs. Kang et al.[77] also reported the remarkably improved conductivity of MnO_2 via atomic doping of Au atom (Figure 7c) and the Au-doped MnO_2 film exhibited substantially improved capacitive performance.

Nanoscale Horizons Accepted Manuscript

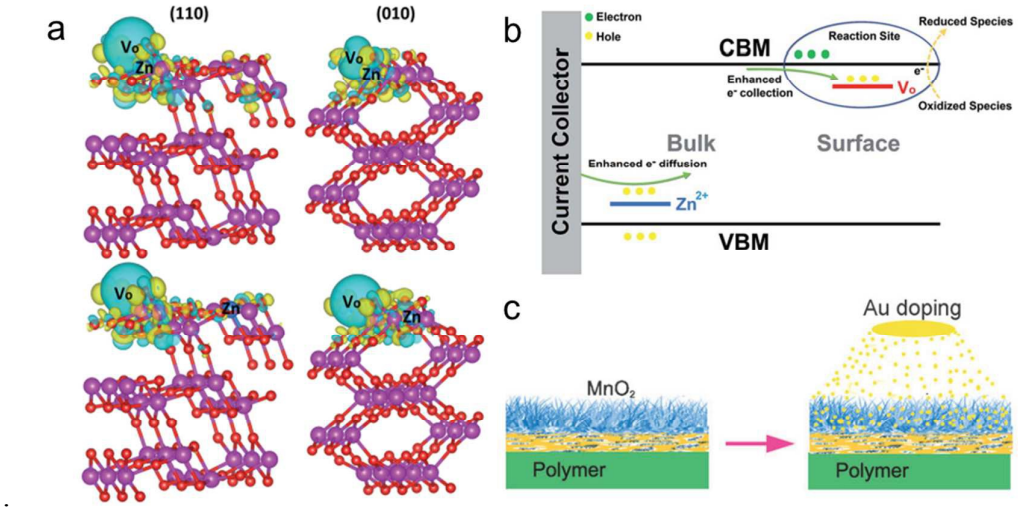

Figure 7. a) The charge density difference of (010) and (110) surfaces of Zn-doped ramsdellite-MnO_2 with the oxygen vacancy of site I. The blue and yellow areas highlight the electron loss and gain, respectively. b) Schematic illustration of the effects on the MnO_2 materials from Zn^{2+} doping. Reprinted from ref.[75] with the permission from Royal Society of Chemistry 2015. c) Sketch of the fabrication process of the Au-doped MnO_2 electrodes. Reprinted from ref.[77] with the permission from 2013 Wiley-VCH Verlag GmbH & Co. KGaA, Weinheim.

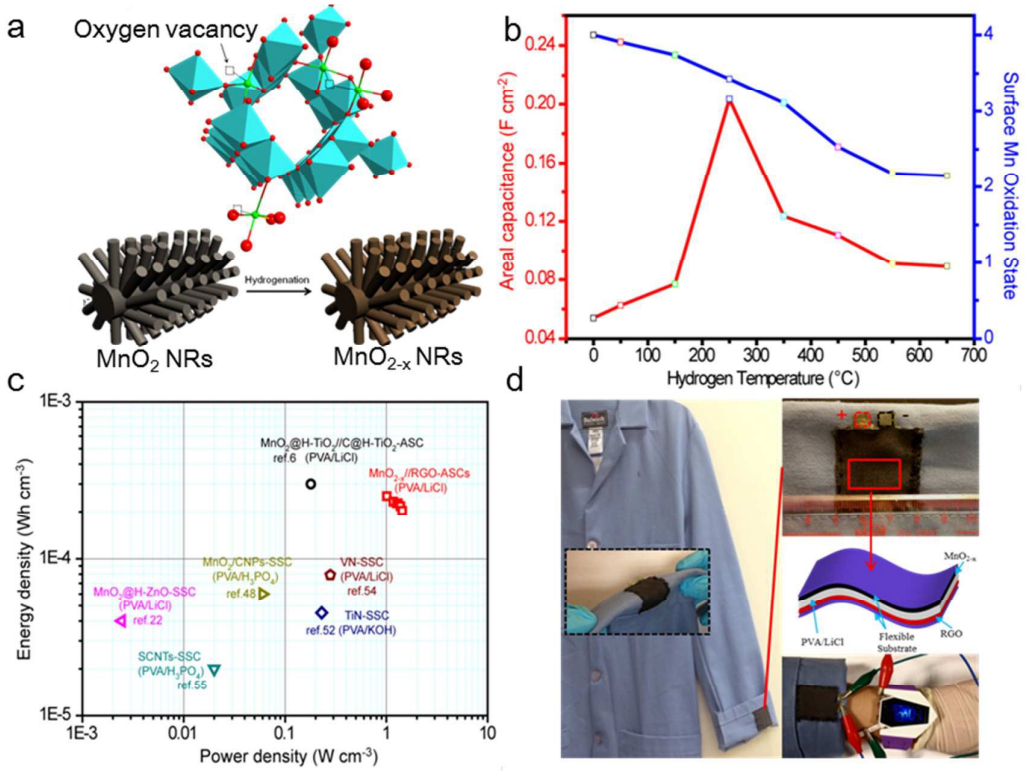

Figure 8. a) Schematic diagram illustrates the growth process for preparing hydrogenated MnO_2 (H-MnO_2) NRs on carbon cloth substrate. b) Areal capacitance and surface Mn oxidation state of

Nanoscale Horizons Accepted Manuscript

H-MnO_2 as a function of hydrogenated temperature. c) Ragone plots of the H-MnO_2 //RGO ASC device measured in the gel electrolyte. The values reported for other SC devices are added for comparison. d) Photo images of clothes model and zoom-in of wearable ASCs sewing on the clothes model. Reproduced from the ref. [36] with the permission from 2014 Elsevier Ltd.

Annealing in de-oxygen or reducing ambient is the second effective approach for the introduction of oxygen vacancies to MnO_2.[36, 70] Zhai *et al.* demonstrated an effective strategy, annealed the MnO_2 in hydrogen atmosphere (Figure 8a), to intrinsically improve the conductivity and capacitive performance of MnO_2 by inducing oxygen vacancies.[36] Figure 8b shows the areal capacitance and surface Mn oxidation state of hydrogenated MnO_2 (H-MnO_2) as a function of hydrogenated temperature. It could be observed that the H-MnO_2 samples exhibit higher areal capacitance in comparison with the untreated MnO_2 sample. Moreover, H-MnO_2 hydrogenated at 250 °C with moderate oxygen vacancies exhibits the highest areal capacitance of 0.22 F/cm^2 (449 F/g) at 0.75 mA/cm^2. Significantly, a solid-state ASC based on the H-MnO_2 and reduced graphene oxide was assembled and exhibited higher energy density and power density (0.25 mWh/cm^3 at 1.01 W/cm^3) over other reported SCs device (Figure 8c). Finally, to test the feasibility of H-MnO_2//RGO ASC device as energy storage device in wearable electronics, the as-fabricated flexible ASC was knitted into laboratory clothing as a demonstration (Figure 8d).

3.2 Extrinsically modified MnO_2 electrode for flexible SCs

In addition to intrinsically modification of MnO_2, the extrinsically combination of MnO_2 with highly conductive materials, such as carbon based materials,[78-82] metal oxide or conductive polymer based materials,[83-85] has also been investigated extensively for flexible SCs. As the flexible SCs raised critical requirements to these highly conductive supports, the supports for MnO_2 are required to be with high mechanical integrity upon bending or folding and lightweight property as well as with excellent electrochemical properties.[86] Herein, we review in detail the MnO_2 materials grown on non-3D and 3D conductive and flexible supports for flexible SCs.

3.2.1 Non-3D scaffold supported MnO_2 for flexible supercapacitors

Nanoscale Horizons Accepted Manuscript

To meet the demands of flexible supercapacitors, several kinds of non-3D supports including CNT or graphene paper,[78, 80, 87, 88] carbon fabrics,[84, 85, 89] polyethylene terephthalate (PET), transition metal oxide or conductive polymer nanowires,[38, 85] are possible choices for flexible supercapacitor electrodes. Table 1 summarized the typical results of capacitive performance of electrode and SCs based on different platform supports. Though good capacitive performance have been achieved as well as the outstanding flexibility, the low surface area of these flat supports limited the further improvements to high power and energy density for flexible SCs.

Nanoscale Horizons Accepted Manuscript

Table 1 Typical results of capacitive performance of electrode and SCs based on different platform supports.

Active materials	Conductive scaffold	Capacitance	Mass loading	Flexibility (capacitance retention%)	Energy density retention of SCs	Energy density(E)	Power density (P)	Cycle stability	Ref.
MnO_2	Graphene/ CNT paper	486.6 F/g at 2 mV/s	--	Negligible variation of electrical conductivity (1000 bending cycles)	~40% (Power density form 150 to 2250 W/kg)	24.8 Wh/kg	~150 W/kg	--	Ref.[80]
MnO_2	3D hollow structured graphene	~280 F/g at 2 mV/s	0.42 mg/cm^2	92% (200 bending cycles)	~55% (P form 62 to 2500 W/kg)	6.8 Wh/kg	62 W/kg	81.2% after 5000 cycles	Ref.[78]
MnO_2	3D graphene/CNT	343.1 F/g at 2 mV/s,	0.21 mg/cm^2	--	~ 56.8% (P form 170.5 to 22727 W/kg)	33.71 Wh/kg	170.5 W/kg	95.3% after 1000 cycles.	Ref.[90]
MnO_2	Graphene foam	422.5 F/g at 1 A/g	--	~97% after bending 180° for 100 times.	~ 57.2% (P form 453.6 to 9188.1 W/kg)	31.8 Wh/kg	453.6 W/kg	84.4% after 10000 cycles	Ref.[82]
MnO_2	H-TiO_2 nanowires@ carbon cloth	449.6 F/g at 10 mV/s	0.23 mg/cm^2	Negligible variation at twisted and bending states	~ 56.7% (P form 35000 to 45000 W/kg)	0.30 mWh/cm^3 (59 Wh/kg)	0.23 W/cm^3 (45 kW/kg)	91.2% after 5000 cycles	Ref.[85]
MnO_2 nanorod	Graphene film	209 F/g at 1 mVs	--	~97.2% at the bent states	~ 24% (P form 101.5 to 24500 W/kg)	50.8 Wh/kg	101.5 W/kg	81% after 1000 cycles	Ref.[87]

Nanoscale Horizons Accepted Manuscript

MnO_2	Few walled CNT paper	203 F/g at 2 mV/s	--	--	89% (P form 130 to 7800 W/kg)	23.9 Wh/kg	7.8 kW/kg	95% after 2000 cycles	Ref.[88]
Ppy/MnO_2	Carbon fiber	--	--	99.76% when it was rolled up	~ 26% (P form 0.05 to 2 W/cm^3)	6.16 mWh/cm^3	0.05 W/cm^3	86.7% after 1000 cycles	Ref.[84]
MnO_2	CNF paper	525 mF/cm^2 (110 F/g) at 3 mA cm^2	3.1 mg/cm^2	Yes	80.5% (P form 352.6 to 3370 W/kg)	43.4 $\mu Wh/cm^2$ (11.3 Wh/kg)	1.35 mW/cm^2 (352.6 W/kg)	85% after 4000 cycles	Ref.[25]
$CuCo_2O_4$@ MnO_2 nanowire	carbon fabrics	327 F/g at 1.25 A/g	0.5 mg/cm^2	No significant deviations at 0, 30, 60, 90°	70% (P form 0.4745 to 3120 mW/cm^2)	94.3 Wh/cm^2	0.4757 mW/cm^2	long-term cycling life over 3000 cycles in different bent states.	Ref.[89]
MnO_2	polyethylene terephthalate	4.72 mF/cm^2 at 5$\mu A/cm^2$	--	SC No obvious change bent at 0 90°	--	--	--	85.5% capacitance retention after 500 cycles	Ref.[91]
Ppy/MnO_2	CNT textile	461.0 F/g at 0.2 A/g	--	SC 96.2% of initial value after 750 000 bending cycles,	--	31.1 Wh/kg	22.1 kW/kg	93.8% capacitance retention after 10000 cycles	Ref.[92]
MnO_2	stainless steel mesh	667 F/g at 5 mV/s	--	--				--	Ref.[93]

Nanoscale Horizons Accepted Manuscript

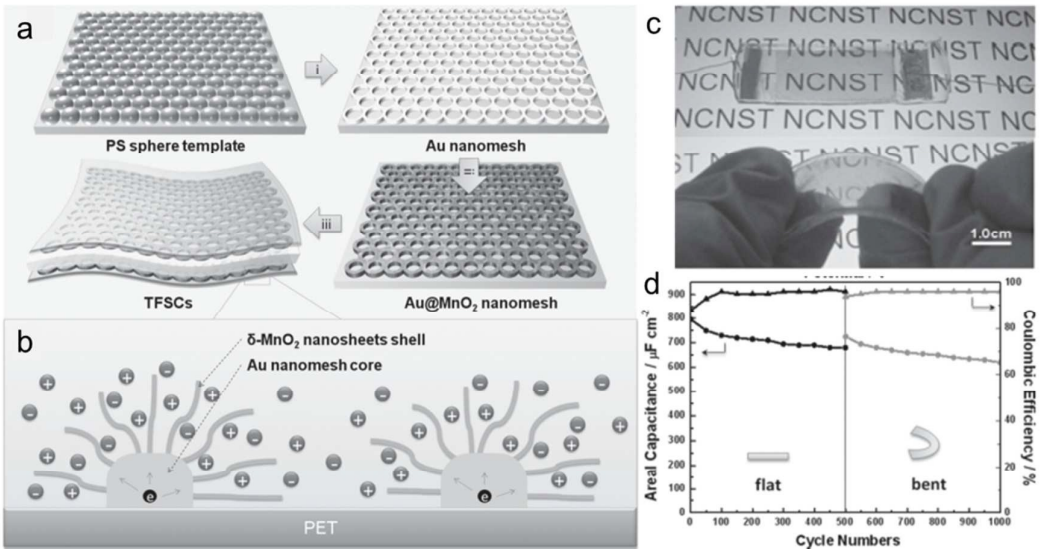

Figure 9. a) Schematic illustration for the fabrication of flexible SCs based on the Au@MnO_2 nanomesh. b) Schematic diagram of ion diffusion pathways and charge transport channels of the Au@MnO_2 nanomesh electrode. c) Photo images of the Au@MnO_2 nanomesh electrode based SCs sealed in a PDMS film, flat and bent. d) cyclic stability and coulombic efficiency of the device at flat and bending state. Reprinted from ref.[91] with the permission from 2014 Wiley-VCH Verlag GmbH & Co. KGaA, Weinheim.

Qiu and his co-workers [91] recently developed the first time a novel Au@MnO_2 core-shell nanomesh structure on a flexible polymeric substrate. Figure 9a shows the illustration for the fabrication of flexible SCs based on the flexible Au@MnO_2 nanomesh electrode. The average diameter of the applied polystyrene (PS) particle is around 700 nm and the as prepared Au nanomesh film with a thickness of 50 nm achieved a sheet resistance of 13~18 Ω/sq, indicating the higher surface area (compared with platform supports) and good conductivities. Moreover, a flexible SC (Figure 9c) based on the Au@MnO_2 nanomesh electrode was assembled to explore the advantages of this novel design. A stable coulombic efficiency of greater than 95% over 1000 cycles was obtained at flat and bent states, indicating the stable Au nanomesh supports and strong coupling between the Au nanomesh and MnO_2 nanosheets. However, the surface area of Au nanomesh flexible supports still cannot compare with the one-dimensional (1D) nanostructured supports. Meanwhile, the use of Au may hinder the wide application of the Au nanomesh. Lu *et al*. [85] developed a

Nanoscale Horizons Accepted Manuscript

high-performance and flexible solid-state ASC devices based on 1D core-shell nanowire (NW) electrodes (Figure 10a). The hydrogen-treated TiO_2 (denoted as H-TiO_2) NWs was adopted as the core (conducting scaffold) to support electrochemically active MnO_2. Figure 10b presents the CV curves collected for H-TiO_2, MnO_2, TiO_2@MnO_2 and H-TiO_2@MnO_2 electrodes at the scan rate of 100 mV/s. Obviously, the H-TiO_2@MnO_2 electrode exhibits substantially higher current density than the values obtained for the MnO_2 and TiO_2@MnO_2 electrodes, which can be attributed to the increased surface area through the H-TiO_2 nanostructured supports and the enhanced charge transport for TiO_2 after hydrogenation. As the scan rate increased from 10 to 200 mV/s, the H-TiO_2@MnO_2 electrode retained 54.6% of its capacitance, which is also substantially higher than that of the MnO_2 (29.4%) and TiO_2@MnO_2 (43.4%) electrodes, again confirming the enhanced charge transport during the charge/discharge process. Moreover, the electrode materials directly grown on carbon cloth enable the ASC device with outstanding flexibility (Figure 10d). The as assembled flexible ASC device delivered a maximum energy density of 0.30 mW h/cm^3 (59 Wh/ kg) (Figure 10e), which is higher than most of the reported SSCs.[11, 79, 94, 95]

Nanoscale Horizons Accepted Manuscript

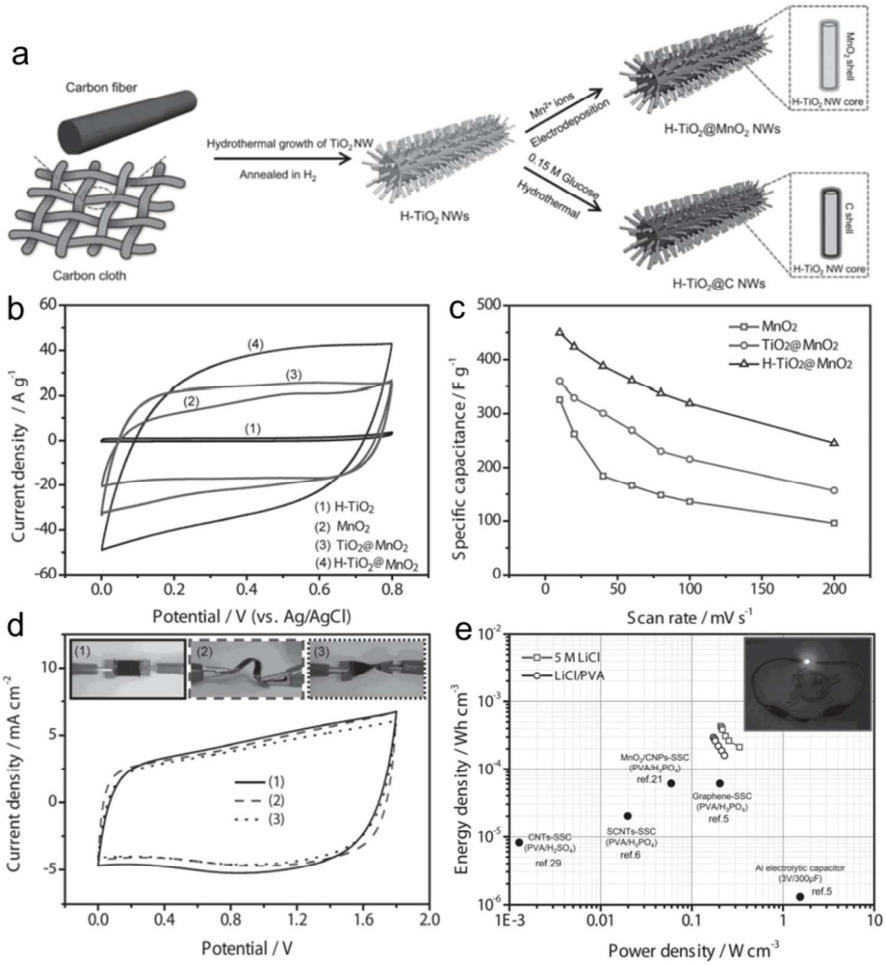

Figure 10. a) Schematic diagram illustrating the growth processes for H-TiO_2@MnO_2 and H-TiO_2@C core–shell NWs on a carbon cloth substrate. b) CV curves collected for H-TiO_2, MnO_2, TiO_2@MnO_2 and H-TiO_2@MnO_2 electrodes at the scan rate of 100 mV/s. c) Specific capacitance of these electrodes as a function of scan rates. d) CV curves collected at a scan rate of 100 mV/s for the ASC device under flat, bent, and twisted conditions. Insets are the device pictures under test conditions. e) Ragone plots of the ASC devices measured in the aqueous and gel electrolyte. The values reported for other SC devices are added for comparison. Reprinted from ref. [85] with the permission from 2013 Wiley-VCH Verlag GmbH & Co. KGaA, Weinheim.

Similar with other transition metal oxides, the MnO_2 also suffer from the delamination problems caused by the large volume changes during charge/discharge cycles, and hence a decrease in electrochemical stability.[96, 97] To prevent the delamination of nanostructured MnO_2 electrodes, researchers have tried to coat a thin conductive layer on the top of MnO_2.[92, 98] Yun *et al.* [92] used the polypyrrole (Ppy) conductive polymer to coat on the top of MnO_2 nanoparticles to prevent the

Nanoscale Horizons Accepted Manuscript

delamination (Figure 11a). With the protected conductive polymer layer, the Ppy-MnO_2/CNT electrode achieved improved cycling stability, with 93.8% normalized capacitance after 10 000 cycles (Figure 11b), which is higher than that of MnO_2/CNT electrode. Significantly, the Ppy-MnO_2/CNT based SCs exhibited excellent flexibility (Figure 11c). As shown in Figure 11d, the Ppy-MnO_2/CNT based SCs still well retained the almost original capacitive performance even after 750 000 bending cycles, with capacity retention of 98.9, 98.4, and 96.2% of initial value after 250 000, 500 000, and 750 000 bending cycles, respectively.

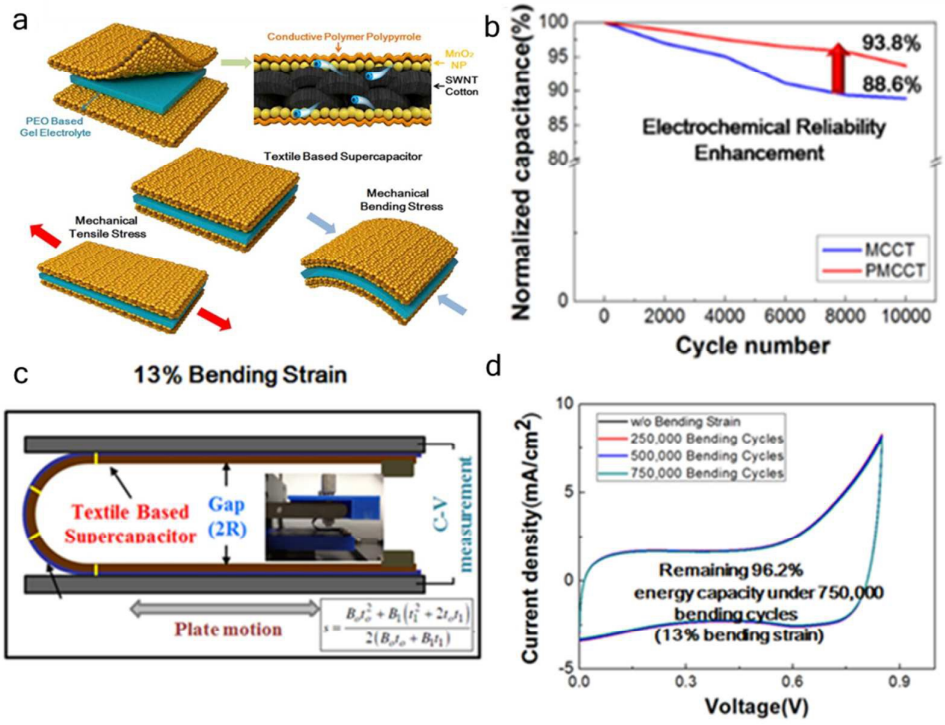

Figure 11. a) Schematic illustration of Ppy-MnO_2-coated textile SC. b) Cycling stability of the Ppy-MnO_2-coated textile electrode c) Schematic for bending test performed on Ppy-MnO_2-coated textile SC. (d) CV cureves of supercapacitor under 13% bending strain collected at 0, 250 000, 500 000, 750 000 bending cycles. Reprinted from ref.[92] with permission from Copyright © 2015, American Chemical Society.

3.2.2 3D scaffold supported MnO_2 for flexible supercapacitors

The design of 3D architectures for electrodes has been considered as a highly

Nanoscale Horizons Accepted Manuscript

efficient approach because of is ability to reduce "dead surface" of active materials, porous channels facilitated ionic diffusion process. In recent years, 3D constructed MnO_2 electrodes attract particular interest when compared to lower dimensional structures.[99] The 3D constructed MnO_2 electrodes usually consist of MnO_2 active materials and conductive 3D scaffold assembled from low-dimensional units (including one or more types of 0D, 1D, 2D nanomaterials), which can retain the intrinsic properties of the low-dimensional structure as well as faster and more efficient electronic, ionic transport. Graphene based 3D architectures are one of the most used flexible 3D scaffolds for MnO_2 based SCs owing to the graphene resulted high conductivity, high surface area. In addition, its lightweight feature resulted high active mass ratio is quite meaningful for SC at practical application. For example, Zhai *et al.* [100] developed an electrochemical capacitor using highly conductive 3D graphene hollow (3DGH) structure (Figure 12a) as current collector to pursue high active material ratio for MnO_2 based cathode and V_3S_4 anode. The as prepared 3DGH exhibited an outstanding flexibility (Figure 12b). Finally, the V_3S_4@3DGH and MnO_2@3DGH were assembled into a ASC (Figure 12c) with high active material ratio of 24% and delivered a remarkable energy density of 7.4 Wh/kg (based on the weight of entire device) at the average power density of 3000 W/kg. He and his co-workers [78] also fabricated a flexible symmetrical SC (of weight less than 10 mg and thickness ~ 0.8 mm; Figure 12d) consisting of a sandwich structure of two pieces of 3D graphene/MnO_2 composite network. The 3D graphene network facilitates the synthesis of electrodes with high active material ratio (~ 92.9% of the mass of entire electrode). Moreover, the 3D graphene/MnO_2 composite network-based symmetrical SC delivered an acceptable cycling stability performance even at bending angle of 90° (Figure 12e). It should be noted that the mass loading of active materials for 3D graphene network to assemble into flexible SC is usually limited at ~ 1 mg/cm^2.[78, 100] The electrode will be more rigid at high active materials loading level, which will severely limited its further progress. Xia *et al.* [101] reported a new type of 3D porous and thin graphite foams (GF) as the light and conductive substrates for the growth of metal oxide core/shell nanowire arrays to form integrated electrodes. The porous GF

Nanoscale Horizons Accepted Manuscript

possesses a porosity of ~ 99.8% and a super high surface area of ~ 980 m^2/g, which result in its lightweight (~ 4 mg/cm^3) and excellent scaffold for active materials (Figure 13 a-d). In addition to its excellent conductivity, the GF based electrode presents high specific capacitance (based on the mass of the whole weight of the electrode), good rate capability, and further enhanced energy/power density (Figure 13e).

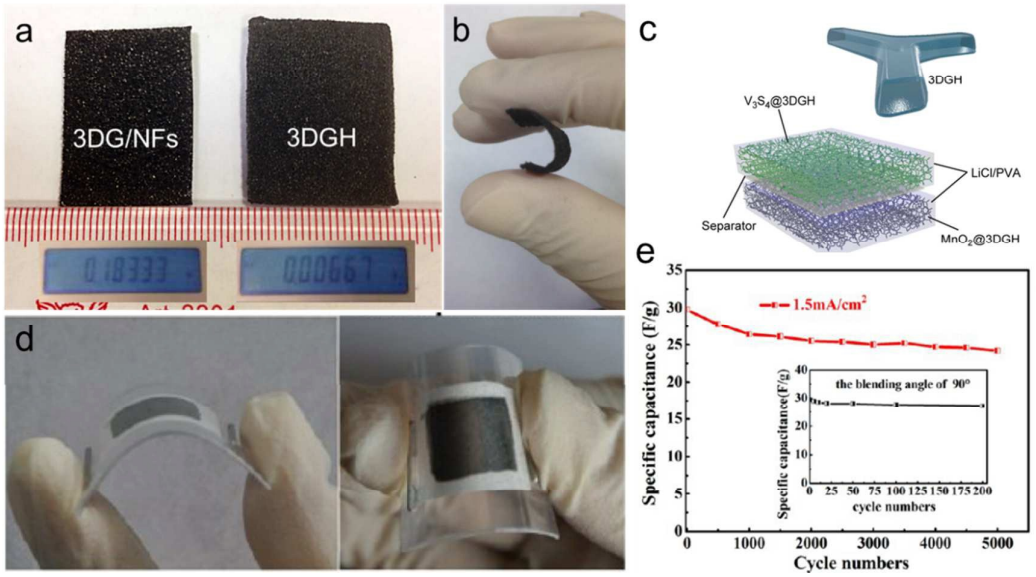

Figure 12. a) Photo images of 3D graphene/Ni foams (3DG/NFs) and 3D hollow graphene (3DGH) samples. The insets are the mass of each sample (sample area, 6 cm^2). b) Illustration of the flexibility of 3DGH sample. c) A schematic illustration of V_3S_4/3DGH//MnO_2/3DGH device. Reprinted from ref.[100] with permission from Copyright © 2015, American Chemical Society. d) digital photographs shown the flexible SC at bent states. e) Cycling stability of the as assembled flexible SC collected at a current density of 1.5 mA/cm^2 for 5000 cycles. Inset shows its cycling performance for bending cycles with a bending angle of 90°. Reprinted from ref.[78] with permission from Copyright © 2012, American Chemical Society.

Nanoscale Horizons Accepted Manuscript

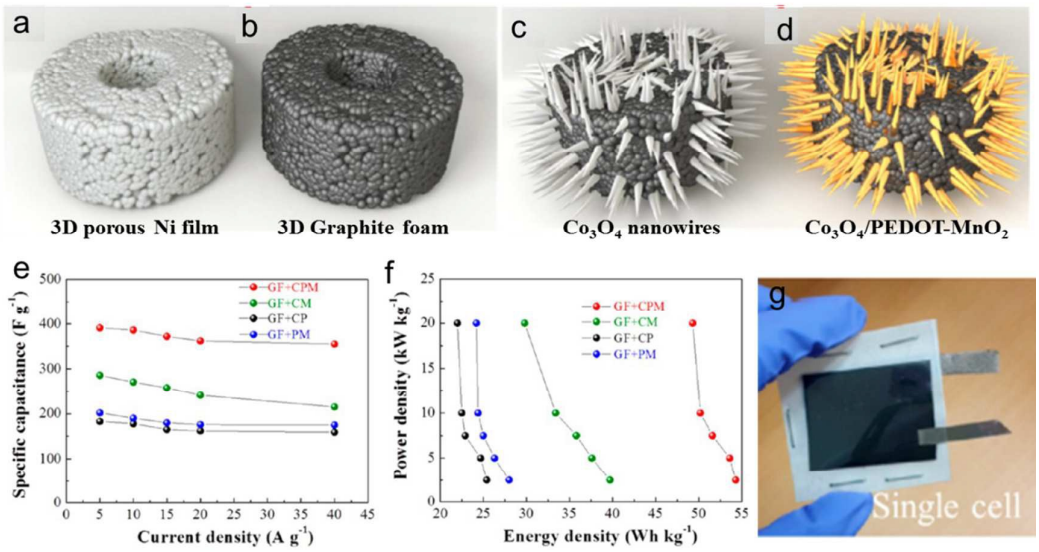

Figure 13. a)-d) Schematics of the fabrication process of thin 3D porous graphite foams (GF) and GF based Co_3O_4/PEDOT-MnO_2 core/shell nanowire arrays. (e) Specific capacitance of four positive electrodes as a function of current densities (It should be noted that the capacitance of the positive electrode is calculated based on the mass of the whole electrode). (f) Ragone plot of four positive electrodes. g) Photos of as assembled flexible asymmetric supercapacitor device. Reprinted from ref.[101] with permission from Copyright © 2014, American Chemical Society.

4. Summary and prospective

Intensive interests have been stimulated to the Manganese oxide (MnO_2) for flexible supercapacitors owing to its outstanding features such as low-cost, high theoretical capacitance, and wide working potential window. However, one of the crucial challenges for MnO_2 as electrode for flexible supercapacitors is the poorly electronic and ionic conductivities, which have hindered their wider application in SCs. To overcome this challenge, intensively works have been devoted. In this review, recent advances in intrinsically and extrinsically modified MnO_2 have been summarized, including the approach to tune the crystallinity, synthesis of MnO_2 with certain targeted crystal structure, oxygen vacancy introduction, construction of flexible non-3D and 3D architecture composites. The integration of MnO_2 to low-dimensional supports with high surface area, and highly conductive, flexible 3D scaffold could achieve high specific capacitance close to the theoretical value and

Nanoscale Horizons Accepted Manuscript

good rate capability. While, the mass loading of MnO_2 in most of reports are limited below 1 mg/cm^2, which is meaningless to flexible SC at practical level since a super low volumetric capacitance will be resulted in. Moreover, the interfacial problems between the MnO_2 and the conductive support are still rarely investigated. For the introduction of oxygen vacancy into MnO_2, the electronic conductivity is enhanced significantly. However, the concentration of oxygen vacancy cannot be introduced controllably. In particular, there is still lack of a facile, efficient method to introduce the oxygen vacancy into bulk MnO_2 instead of just surface. Given these unresolved problems or challenges, the following aspects might be possible ways to develop really applicable MnO_2 electrodes with ultrahigh energy density and power density for flexible SCs:

1. The mass loading of commercial level (~10 mg/cm^2) for MnO_2 active materials has already been achieved via varied approach.[17, 102] However, the specific capacitance are still too far from the theoretical value (~1370 F/g), *i.g.*, MnO_2/Graphene gel/NF (234 F/g, 13.61 mg/cm^2, 10 mV/s),[17] graphene-MnO_2 composites (147 F/g, 9.6 mg/cm^2, 2 mV/s),[78] MnO_2-CNT-textile (337 F/g, 8.3 mg/cm^2, 0.05 mV/s),[102] MnO_2-PEDOT:PSS composites (196 F/g, 8.5 mg/cm^2, 0.5 mA/cm^2),[103] even comparable with commercial activated carbon. The integration with high-surface area carbon or other conductive materials is a common approach for MnO_2 to achieve high capacitive performance at high mass loading level. However, since the limitation of MnO_2 with high mass loading is the electronic transport in its phase, the intrinsically modification should be the efficient way. In this regard, further investigation might better be focused on the oxygen vacancy introduction to pursue fast electronic transport and high capacitance at high mass loading level.
2. Oxygen vacancy, as one of the most efficient method to intrinsically improve the electronic conductivities, has drawn intensively attention in recent years. Varied approaches including annealed in de-oxygen atmosphere, atomic or ion doping are adopted to introduce oxygen vacancy into the MnO_2 active materials. Enhanced

Nanoscale Horizons Accepted Manuscript

electrochemical properties for MnO_2 have been achieved by the oxygen vacancy introduction. However, these kinds of methods can only introduce the deficiency into the surface area of MnO_2. With respect to MnO_2 at high mass loading, the oxygen vacancy does limited contribution to the electrochemical performance of the MnO_2 electrodes. Thus, further investigations on new methods to introduce the oxygen vacancy into the bulk or inactive phase of MnO_2 might be of value for MnO_2 based flexible SC.

3. The mechanical property of 3D conductive scaffold is still one of the major concerns for its application in flexible SCs. The flexible, wearable electronics have raised critical requirement such as stretch ability, flexibility, twisted ability to the flexible SCs and also the electrode. Nevertheless, the 3D scaffold for MnO_2 active materials in current studies involves the construction of 3D structure. Its flexibility is usually realized via the impregnation of elastic polymers like PMMA，[78] which will remarkably hinder the electron transport and prevent the porous structure from the electrolyte ions. Therefore, new modifications to existing 3D scaffold such as 3D graphene foam or graphene hydrogel and/or construction of new-type 3D scaffold need to be developed.

Author contributions

The manuscript was written through the contributions of all the authors. All the authors have given approval to the final version of the manuscript.

Conflict of interest

The authors declare no competing financial interest.

Acknowledgements

We acknowledge the nancial support of this work received by the Natural Science Foundation of China (21403306 and 21273290), Guangdong Province Natural

Nanoscale Horizons Accepted Manuscript

Science Foundation for Distinguished Young Project (2014A030306048), Foundation for Youth Innovative Talents in Higher Education of Guangdong (2014KQNCX003) and The Research Foundation of IARC-SYSU (201408).

References

1. T. Mahlia, T. Saktisahdan, A. Jannifar, M. Hasan and H. Matseelar, *Renewable and Sustainable Energy Reviews*, 2014, **33**, 532-545.
2. M. I. Hoffert, K. Caldeira, G. Benford, D. R. Criswell, C. Green, H. Herzog, A. K. Jain, H. S. Kheshgi, K. S. Lackner and J. S. Lewis, *science*, 2002, **298**, 981-987.
3. P. Simon, Y. Gogotsi and B. Dunn, *Science*, 2014, **343**, pp. 1210-1211.
4. G. Wang, L. Zhang and J. Zhang, *Chem. Soc. Rev.*, 2012, **41**, 797-828.
5. B. E. Conway, *Electrochemical supercapacitors: scientific fundamentals and technological applications*, Springer Science & Business Media, 2013.
6. B. D. Gates, *science*, 2009, **323**, 1566-1567.
7. X. Lu, M. Yu, G. Wang, Y. Tong and Y. Li, *Energy Environ. Sci.*, 2014, **7**, 2160-2181.
8. J. R. Miller and P. Simon, *Science* , 2008, **321**, 651-652.
9. M. D. Stoller, S. Park, Y. Zhu, J. An and R. S. Ruoff, *Nano Lett*, 2008, **8**, 3498-3502.
10. H. M. Jeong, J. W. Lee, W. H. Shin, Y. J. Choi, H. J. Shin, J. K. Kang and J. W. Choi, *Nano Lett.*, 2011, **11**, 2472-2477.
11. M. F. El-Kady, V. Strong, S. Dubin and R. B. Kaner, *science*, 2012, **335**, 1326-1330.
12. K. H. An, W. S. Kim, Y. S. Park, Y. C. Choi, S. M. Lee, D. C. Chung, D. J. Bae, S. C. Lim and Y. H. Lee, *Adv Mater*, 2001, **13**, 497-500.
13. D. N. Futaba, K. Hata, T. Yamada, T. Hiraoka, Y. Hayamizu, Y. Kakudate, O. Tanaike, H. Hatori, M. Yumura and S. Iijima, *Nat. Mater.*, 2006, **5**, 987-994.
14. J. Gamby, P. Taberna, P. Simon, J. Fauvarque and M. Chesneau, *J Power Sources*, 2001, **101**, 109-116.
15. K. Naoi and P. Simon, *Interface*, 2008, **17**, 34-37.
16. J. Cao, X. Li, Y. Wang, F. C. Walsh, J.-H. Ouyang, D. Jia and Y. Zhou, *J Power Sources*, 2015, **293**, 657-674.
17. T. Zhai, F. Wang, M. Yu, S. Xie, C. Liang, C. Li, F. Xiao, R. Tang, Q. Wu and X. Lu, *Nanoscale*, 2013, **5**, 6790-6796.
18. J. Wei, N. Nagarajan and I. Zhitomirsky, *J Mater. Process. Tech.*, 2007, **186**, 356-361.
19. S. Park, H.-W. Shim, C. W. Lee, H. J. Song, I. J. Park, J.-C. Kim, K. S. Hong and D.-W. Kim, *Nano Research*, 2015, **8**, 990-1004.
20. A. Boisset, L. Athouel, J. Jacquemin, P. Porion, T. Brousse and M. r. m. Anouti, *J. Phys. Chem. C*, 2013, **117**, 7408-7422.
21. H. Y. Wang, F. X. Xiao, L. Yu, B. Liu and X. W. D. Lou, *small*, 2014, **10**, 3181-3186.
22. L. Peng, X. Peng, B. Liu, C. Wu, Y. Xie and G. Yu, *Nano Lett.*, 2013, **13**, 2151-2157.
23. S. Devaraj and N. Munichandraiah, *J. Phys. Chem. C*, 2008, **112**, 4406-4417.

Nanoscale Horizons Accepted Manuscript

24. L. Athouël, F. Moser, R. Dugas, O. Crosnier, D. Bélanger and T. Brousse, *J. Phys. Chem. C*, 2008, **112**, 7270-7277.
25. H. Xu, X. Hu, H. Yang, Y. Sun, C. Hu and Y. Huang, *Adv. Energy Mater.*, 2015, **5**, 1401882.
26. P. Yang, Y. Ding, Z. Lin, Z. Chen, Y. Li, P. Qiang, M. Ebrahimi, W. Mai, C. P. Wong and Z. L. Wang, *Nano Lett*, 2014, **14**, 731-736.
27. P. Yang, Y. Li, Z. Lin, Y. Ding, S. Yue, C. P. Wong, X. Cai, S. Tan and W. Mai, *J Mater. Chem. A*, 2014, **2**, 595-599.
28. F. Lai, Y.-E. Miao, Y. Huang, T.-S. Chung and T. Liu, *J. Phys. Chem. C*, 2015, **119**, 13442-13450
29. X. Li, G. Wang, X. Wang, X. Li and J. Ji, *J. Mater. Chem. A*, 2013, **1**, 10103-10106.
30. P. Xu, B. Wei, Z. Cao, J. Zheng, K. Gong, F. Li, J. Yu, Q. Li, W. Lu and J.-H. Byun, *ACS nano*, 2015, **9**, 6088–6096
31. H. Xu, X. Hu, Y. Sun, H. Yang, X. Liu and Y. Huang, *Nano Research*, 2015, **8**, 1148-1158.
32. Y. Huang, Y. Li, Z. Hu, G. Wei, J. Guo and J. Liu, *J. Mater. Chem. A*, 2013, **1**, 9809-9813.
33. J. A. Dawson and I. Tanaka, *ACS applied materials & interfaces*, 2014, **6**, 17776-17784.
34. D. A. Tompsett, S. C. Parker and M. S. Islam, *J. Mater. Chem. A*, 2014, **2**, 15509-15518.
35. J. A. Dawson, H. Chen and I. Tanaka, *ACS appl. Mater.& interf.*, 2015, **7**, 1726-1734.
36. T. Zhai, S. Xie, M. Yu, P. Fang, C. Liang, X. Lu and Y. Tong, *Nano Energy*, 2014, **8**, 255-263.
37. H. Y. Lee and J. B. Goodenough, *J Solid State Chem.*, 1999, **144**, 220-223.
38. X. Lu, T. Zhai, X. Zhang, Y. Shen, L. Yuan, B. Hu, L. Gong, J. Chen, Y. Gao and J. Zhou, *Adv. Mater.*, 2012, **24**, 938-944.
39. X. Lu, D. Zheng, T. Zhai, Z. Liu, Y. Huang, S. Xie and Y. Tong, *Energy Environ. Sci.*, 2011, **4**, 2915-2921.
40. M. Toupin, T. Brousse and D. Bélanger, *Chem. Mater.*, 2004, **16**, 3184-3190.
41. M. J. Young, A. M. Holder, S. M. George and C. B. Musgrave, *Chem. Mate.r*, 2015, **27**, 1172-1180.
42. P. Simon and Y. Gogotsi, *Nat. Mater.*, 2008, **7**, 845-854.
43. Y. T. Weng, H. A. Pan, R. C. Lee, T. Y. Huang, Y. Chu, J. F. Lee, H. S. Sheu and N. L. Wu, *Adv. Energy Mater.*, 2015.
44. Q. Li, X.-F. Lu, H. Xu, Y.-X. Tong and G.-R. Li, *ACS appl. Mater.& interf.*, 2014, **6**, 2726-2733.
45. J. Yan, A. Sumboja, X. Wang, C. Fu, V. Kumar and P. S. Lee, *small*, 2014, **10**, 3568-3578.
46. C.-K. Lin, K.-H. Chuang, C.-Y. Lin, C.-Y. Tsay and C.-Y. Chen, *SuCT*, 2007, **202**, 1272-1276.
47. J.-K. Chang, Y.-L. Chen and W.-T. Tsai, *J Power Sources*, 2004, **135**, 344-353.
48. C. M. Ghimbeu, A. Malak-Polaczyk, E. Frackowiak and C. Vix-Guterl, *J. Appl. Electrochem.*, 2014, **44**, 123-132.
49. S. Donne, A. Hollenkamp and B. Jones, *J Power Sources*, 2010, **195**, 367-373.
50. T. Brousse, M. Toupin, R. Dugas, L. Athouël, O. Crosnier and D. Bélanger, *J. Electrochem. Soc.*, 2006, **153**, A2171-A2180.
51. Y.-C. Chen, Y.-K. Hsu, Y.-G. Lin, Y.-K. Lin, Y.-Y. Horng, L.-C. Chen and K.-H. Chen, *Electrochim. Acta*, 2011, **56**, 7124-7130.
52. Y. Hu, H. Zhu, J. Wang and Z. Chen, *J Alloy. Compd.*, 2011, **509**, 10234-10240.
53. J. Lin, C. Zhang, Z. Yan, Y. Zhu, Z. Peng, R. H. Hauge, D. Natelson and J. M. Tour, *Nano Lett.*, 2012, **13**, 72-78.

Nanoscale Horizons Accepted Manuscript

54. D. Pech, M. Brunet, H. Durou, P. Huang, V. Mochalin, Y. Gogotsi, P.-L. Taberna and P. Simon, *Nat. nanotech.*, 2010, **5**, 651-654.
55. J. Chmiola, C. Largeot, P.-L. Taberna, P. Simon and Y. Gogotsi, *science*, 2010, **328**, 480-483.
56. G. Han, Y. Liu, L. Zhang, E. Kan, S. Zhang, J. Tang and W. Tang, *Sci. rep.*, 2014, **4**.
57. W. Zilong, Z. Zhu, J. Qiu and S. Yang, *J. Mater. Chem. C*, 2014, **2**, 1331-1336.
58. B. You, N. Li, H. Zhu, X. Zhu and J. Yang, *ChemSusChem*, 2013, **6**, 474-480.
59. W. Li, K. Xu, B. Li, J. Sun, F. Jiang, Z. Yu, R. Zou, Z. Chen and J. Hu, *ChemElectroChem*, 2014, **1**, 1003-1008.
60. H. Jiang, T. Zhao, J. Ma, C. Yan and C. Li, *Chem. Commun.*, 2011, **47**, 1264-1266.
61. J. A. Lee, M. K. Shin, S. H. Kim, H. U. Cho, G. M. Spinks, G. G. Wallace, M. D. Lima, X. Lepró, M. E. Kozlov and R. H. Baughman, *Nat. commun.*, 2013, **4**.
62. X. Xiao, T. Li, P. Yang, Y. Gao, H. Jin, W. Ni, W. Zhan, X. Zhang, Y. Cao and J. Zhong, *ACS nano*, 2012, **6**, 9200-9206.
63. X. Wang, B. Liu, R. Liu, Q. Wang, X. Hou, D. Chen, R. Wang and G. Shen, *Angew. Chem.*, 2014, **126**, 1880-1884.
64. K. Jost, D. Stenger, C. R. Perez, J. K. McDonough, K. Lian, Y. Gogotsi and G. Dion, *Energy Environ. Sci.*, 2013, **6**, 2698-2705.
65. Z. Yang, J. Deng, X. Chen, J. Ren and H. Peng, *Angew. Chem. Int. Ed.*, 2013, **52**, 13453-13457.
66. Y. Zhang, W. Bai, X. Cheng, J. Ren, W. Weng, P. Chen, X. Fang, Z. Zhang and H. Peng, *Angew. Chem. Int. Ed.*, 2014, **53**, 14564-14568.
67. T. Chen, R. Hao, H. Peng and L. Dai, *Angew. Chem. Int. Ed.*, 2015, **54**, 618-622.
68. J. Yang, X. Zhou, W. James, S. Malik and C. Wang, *arXiv preprint cond-mat/0409345*, 2004.
69. M.-K. Song, S. Cheng, H. Chen, W. Qin, K.-W. Nam, S. Xu, X.-Q. Yang, A. Bongiorno, J. Lee and J. Bai, *Nano Lett*, 2012, **12**, 3483-3490.
70. F. Cheng, T. Zhang, Y. Zhang, J. Du, X. Han and J. Chen, *Angew. Chem. Int. Ed.*, 2013, **52**, 2474-2477.
71. Y. Li and H. Xie, *Ionics*, 2010, **16**, 21-25.
72. G. Zhang, L. Zheng, M. Zhang, S. Guo, Z.-H. Liu, Z. Yang and Z. Wang, *Energ Fuel*, 2011, **26**, 618-623.
73. Q. Ye, R. Dong, Z. Xia, G. Chen, H. Wang, G. Tan, L. Jiang and F. Wang, *Electrochim Acta*, 2014, **141**, 286-293.
74. L. Mai, H. Li, Y. Zhao, L. Xu, X. Xu, Y. Luo, Z. Zhang, W. Ke, C. Niu and Q. Zhang, *Scientific reports*, 2013, **3**.
75. C. Chen, K. Xu, X. Ji, B. Zhang, L. Miao and J. Jiang, *J. Mater. Chem. A*, 2015, 3, 9909-9914.
76. D. Su, S. Dou and G. Wang, *Scientific reports*, 2014, **4**.
77. J. Kang, A. Hirata, L. Kang, X. Zhang, Y. Hou, L. Chen, C. Li, T. Fujita, K. Akagi and M. Chen, *Angew. Chem.*, 2013, **125**, 1708-1711.
78. Y. He, W. Chen, X. Li, Z. Zhang, J. Fu, C. Zhao and E. Xie, *ACS nano*, 2012, **7**, 174-182.
79. L. Yuan, X.-H. Lu, X. Xiao, T. Zhai, J. Dai, F. Zhang, B. Hu, X. Wang, L. Gong and J. Chen, *ACS nano*, 2011, **6**, 656-661.
80. Y. Jin, H. Chen, M. Chen, N. Liu and Q. Li, *ACS appl. Mater. & interf.*, 2013, **5**, 3408-3416.
81. Y. Cheng, S. Lu, H. Zhang, C. V. Varanasi and J. Liu, *Nano Lett.*, 2012, **12**, 4206-4211.
82. Z. Zhang, F. Xiao, L. Qian, J. Xiao, S. Wang and Y. Liu, *Adv. Energy Mater.*, 2014, **4**,

Nanoscale Horizons Accepted Manuscript

1400064.
83. L. Bao, J. Zang and X. Li, *Nano Lett*, 2011, **11**, 1215-1220.
84. J. Tao, N. Liu, W. Ma, L. Ding, L. Li, J. Su and Y. Gao, *Sci. rep.*, 2013, **3**, 2283.
85. X. Lu, M. Yu, G. Wang, T. Zhai, S. Xie, Y. Ling, Y. Tong and Y. Li, *Adv. Mater.*, 2013, **25**, 267-272.
86. X. Peng, L. Peng, C. Wu and Y. Xie, *Chem. Soc. Rev.*, 2014, **43**, 3303-3323.
87. Y. Shao, H. Wang, Q. Zhang and Y. Li, *J. Mater. Chem. C*, 2013, **1**, 1245-1251.
88. Y. Cheng, H. Zhang, S. Lu, C. V. Varanasi and J. Liu, *Nanoscale*, 2013, **5**, 1067-1073.
89. Q. Wang, J. Xu, X. Wang, B. Liu, X. Hou, G. Yu, P. Wang, D. Chen and G. Shen, *ChemElectroChem*, 2014, **1**, 559-564.
90. W. Chen, Y. He, X. Li, J. Zhou, Z. Zhang, C. Zhao, C. Gong, S. Li, X. Pan and E. Xie, *Nanoscale*, 2013, **5**, 11733-11741.
91. T. Qiu, B. Luo, M. Giersig, E. M. Akinoglu, L. Hao, X. Wang, L. Shi, M. Jin and L. Zhi, *small*, 2014, **10**, 4136-4141.
92. T. G. Yun, B. i. Hwang, D. Kim, S. Hyun and S. M. Han, *ACS appl. Mater. & interf.*, 2015, **7**, 9228-9234.
93. J. S. Kim, S. S. Shin, H. S. Han, L. S. Oh, D. H. Kim, J.-H. Kim, K. S. Hong and J. Y. Kim, *ACS appl. Mater. & interf.*, 2013, **6**, 268-274.
94. M. Kaempgen, C. K. Chan, J. Ma, Y. Cui and G. Gruner, *Nano Lett*, 2009, **9**, 1872-1876.
95. Y. J. Kang, H. Chung, C.-H. Han and W. Kim, *Nanot*, 2012, **23**, 065401.
96. H. Jiang, C. Li, T. Sun and J. Ma, *Chem. Commun.*, 2012, **48**, 2606-2608.
97. A. L. M. Reddy, M. M. Shaijumon, S. R. Gowda and P. M. Ajayan, *Nano Lett.*, 2009, **9**, 1002-1006.
98. G. Yu, L. Hu, N. Liu, H. Wang, M. Vosgueritchian, Y. Yang, Y. Cui and Z. Bao, *Nano Lett.*, 2011, **11**, 4438-4442.
99. M. Yu, W. Qiu, F. Wang, T. Zhai, P. Fang, X. Lu and Y. Tong, *J. Mater. Chem. A*, 2015, **3**, 15792-15823.
100. T. Zhai, X. Lu, H. Wang, G. Wang, T. Mathis, T. Liu, C. Li, Y. Tong and Y. Li, *Nano Lett.*, 2015, **15**, 3189-3194.
101. X. Xia, D. Chao, Z. Fan, C. Guan, X. Cao, H. Zhang and H. J. Fan, *Nano Lett.*, 2014, **14**, 1651-1658.
102. L. Hu, W. Chen, X. Xie, N. Liu, Y. Yang, H. Wu, Y. Yao, M. Pasta, H. N. Alshareef and Y. Cui, *ACS nano*, 2011, **5**, 8904-8913.
103. Z. Su, C. Yang, C. Xu, H. Wu, Z. Zhang, T. Liu, C. Zhang, Q. Yang, B. Li and F. Kang, *J. Mater. Chem. A*, 2013, **1**, 12432-12440.
104. X. Wang and Y. D. Li, *J. Am. Chem. Soc.*, 2002, ***124*** **(12)**, 2880-2881
105. B. Solomon, J. J. Wu, E. Thomsen, J. B. Yang and X. D. Zhou, *ECS Meet. Abstr.*, 2012, **MA2012-02**, 1960.
106. Y. Huang, Y. Y. Li, Z. Q. Hu, G. M. Wei, J. L. Guo and J. P. Liu, *J. Mater. Chem. A*, 2013, **1**, 9809.

Nanoscale Horizons Accepted Manuscript

Nanoscale Horizons Accepted Manuscript